Comparison of Visual Servoing Techniques: Experimental Results

Philippe Martinet

COMPARISON OF VISUAL SERVOING TECHNIQUES: EXPERIMENTAL RESULTS

Philippe Martinet

LASMEA, Université Blaise Pascal, UMR 6602 du CNRS,
63177 Aubière cedex, France
Fax: +33 4 73.40.72.62 and e-mail: martinet@lasmea.univ-bpclermont.fr

Keywords: Position based control, Image based control, Visual servoing.

Abstract

In visual servoing applications, two main approaches were defined by Sanderson and Weiss at the beginning of the eighties: *Position Based Control* and *Image Based Control*. The aim of this article is to present different control laws using these approaches, and discuss the main advantages and disadvantages of both approaches through experimental results. The target object is composed of four non-coplanar characteristic points. From the projection of these four points in the image frame, the estimate of the Pose of the object in the sensor frame is computed using the Dementhon algorithm.

1 Introduction

Sanderson and Weiss in [15] introduced an important classification of visual servo structures based on two criteria: control space and the presence of joint-position feedback. So, in this classification we distinguish two main approaches:

Position Based Control: in this case, image features are extracted from the image and a model of the scene and the target is used to determine the pose of the target with respect to the frame attached to the camera.

Image Based Control: in image based control, the pose estimation is omitted, and the control law is directly expressed in the sensor space (image space).

The state of the art in the field of visual servoing, reported in [3] and [8], shows that *Image Based Control* has been retained as an alternative technique to the *Position Based Control* approach. Generally, many authors consider that the *Image Based Control* approach is better of the two with respect to camera calibration, hand-eye calibration, robot modelling, scene and target modelling, and also with regard to the processing time required to compute the sensor signal. It is clear that the *Image Based Control* approach does not need precise calibration and modelling, because of the closed loop defined in the sensor space. Much work [1, 6, 7, 9, 12] has been done on the camera sensor and the $2D$ space.

The notion of *Task Function* introduced by Samson *et al* in [14], can be used to define a control law in the sensor space. According to this concept, Martinet et *al* in [11] introduce the notion of the $3D$ visual sensor which delivers a $3D$ sensor signal by monocular vision at video rate. Recent progress in pose estimation, location and $3D$ modelling [4, 5] shows that it is not unrealistic to introduce $3D$ visual information in a closed loop control. Using this assumption, control laws can be synthesised using this kind of information as we do directly with the camera sensor. In fact, little work [16] has been done using a $3D$ sensor signal. However, precise calibration and modelling are really useful only in the case where the task to achieve is expressed in Cartesian space. If $3D$ reference signals are learned in real conditions, as in the *Image Based Approach*, the same good results as in the $3D$ *sensor space* are obtained.

In the first part of this paper, the experimental context for the comparison and particularly the scene and the sensor signal which are extracted from images, are presented. In the second and third part, the models of different *interaction matrices* are developed using both *Image based and Position Based* approaches. In the fourth and last part, results obtained with our experimental robotic platform are presented and discussed.

2 Experimental context

2.1 Description of the scene

Figure 1 represents the scene with a 3D object, composed of four characteristic points, and a camera mounted on the end effector of the robot. Three homogeneous transformation matrices can be defined:

$\underline{M}_o$ is the homogeneous matrix between an absolute frame attached to the scene, and the object frame $\mathcal{R}_o$,

$\underline{M}_{c_t}$ is the homogeneous transformation matrix between an absolute frame attached to the scene, and the sensor frame computed at each iteration $\mathcal{R}_{c_t}$,

$\underline{M}_c^*$ is the homogeneous transformation matrix between an absolute frame attached to the scene, and the sensor frame desired at the equilibrium $\mathcal{R}_c^*$.

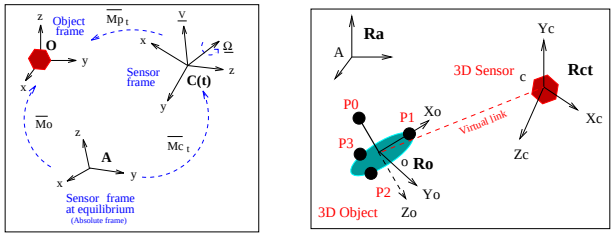

Figure 1: Different frames used in modelling - $3D$ Object

The camera is embedded on the end effector of a Cartesian robot with 6 d.o.f, and connected to the parallel vision system *Windis*. This system is dedicated to visual tracking and visual servoing applications.

2.2 Extraction of sensor signals and camera trajectory estimation

For the purposes of experimentation, a specific vision algorithm based on the DeMenthon algorithm [5] is used. The low level image processing consists in the extraction of the barycenter of each illuminated point in the image space. Using the model of the object, four points from the list of detected points are chosen successively, and the pose of the object $\overline{M}_{p(t)}$ in the sensor frame is computed. The best matching point in image space which corresponds to the best matching in Cartesian space is selected. So, at each iteration (twice video rate), the pose of the object in the sensor frame and four feature points in the image space are selected. From this information, the necessary sensor signals used in the different control laws are computed. For instance, the $3D$ coordinates of each characteristic point, or the pose of the camera $\overline{M}_{C_t}$ in the absolute frame can be extracted with the following relation:

$$\overline{M}_{C_t} = \overline{M}_o . \overline{M}_{p(t)}^{-1} \tag{1}$$

In this relation, estimation of the matrix $\overline{M}_o$ is necessary. This step is realized by a learning phase using all the whole real measurement process.

To estimate the trajectory of the camera during servoing, the use of joint measurement and the geometric model of the robot have been retained. In this condition, the pose of the robot basis in the absolute frame has also to be learned.

3 Image based visual servoing

Consider a $3D$ point M with the following coordinates $(X, Y, Z)^T$ in the sensor frame, and then define the coordinates $\underline{s} = (u, v)^T = (F_u \cdot \frac{X}{Z}, F_v \cdot \frac{Y}{Z})^T$ of the projection of the point M in image space, where F_u and F_v represent the focal length parameters of the camera. In this case, the *image jacobian* (or *interaction matrix*) $L_{\underline{s}}^T$ for the point feature can be established:

$$\begin{pmatrix} -\frac{F_u}{Z} & 0 & \frac{u}{Z} & \frac{uv}{F_v} & -(F_u + \frac{u^2}{F_u}) & v\frac{F_u}{F_v} \\ 0 & -\frac{F_v}{Z} & \frac{v}{Z} & (F_v + \frac{v^2}{F_v}) & -\frac{uv}{F_u} & -u\frac{F_v}{F_u} \end{pmatrix}$$

$L_{\underline{s}}^T$ links the variations of the sensor signal to the kinematic screw applied to the camera Tc, through the relation $(\dot{u}, \dot{v})^T = L_{\underline{s}}^T \cdot Tc$. In our scene, a sensor signal $\underline{S} = (u_0, v_0, u_1, v_1, u_2, v_2, u_3, v_3)^T$, corresponding to the projection of the four characteristic points $\underline{\mathcal{P}}_0$, $\underline{\mathcal{P}}_1$, $\underline{\mathcal{P}}_2$, and $\underline{\mathcal{P}}_3$, has to be considered. Then, the global image jacobian can be written as $L_{\underline{S}}^T = (L_{\underline{s}_0}, L_{\underline{s}_1}, L_{\underline{s}_2}, L_{\underline{s}_3})^T$. The control law uses the *Task Function Approach* [14] introduced at the end of the eighties, and can be defined by the relation:

$$Tc = -\lambda \cdot L_{\underline{S}}^{T^+} \cdot (\underline{S} - \underline{S}^*) \tag{2}$$

In this relation, $\underline{S}^*$ represents the value of the sensor signals at the equilibrium situation, and λ the gain of the control law. For the term $L_{\underline{S}}^{T^+}$, two estimates are possible: the approximation of the value at the equilibrium situation $L_{\underline{S}=\underline{S}^*}^{T^+}$, or the estimation $L_{\underline{S}(t)}^{T^+}$ at each iteration (an estimate of the depth of every point is needed).

4 Position based visual servoing

In this paper, two main models are proposed : the *interaction matrix* for both the $3D$ point feature and *Pose* feature, and a new modelling which presents the advantage that it suppresses the coupling between position control and orientation control.

4.1 First model

In previous papers [11] [10], the method of obtaining the corresponding *interaction matrix* for the $3D$ point feature and *Pose* feature was described.

For the $3D$ point feature $\underline{s} = (\underline{\mathcal{P}})$, the corresponding *interaction matrix* is given by:

$$L_{\underline{s}}^T = [-I_3, AS(\underline{\mathcal{P}})] \tag{3}$$

where $AS(\underline{\mathcal{P}})$ represents the antisymmetric matrix associated with the vector $\underline{\mathcal{P}}$. Considering four characteristic points $\underline{\mathcal{P}}_0$, $\underline{\mathcal{P}}_1$, $\underline{\mathcal{P}}_2$, and $\underline{\mathcal{P}}_3$, the global *interaction matrix* is expressed by $L_{\underline{S}}^T = (L_{\underline{\mathcal{P}}_0}, L_{\underline{\mathcal{P}}_1}, L_{\underline{\mathcal{P}}_2}, L_{\underline{\mathcal{P}}_3})^T$.

For the Pose feature, the sensor signal $\underline{S} = (\underline{X}^T, \underline{\theta}^T)^T$ (dim 6) represents the position and the orientation of the object frame relative to the sensor frame. Then, the corresponding *interaction matrix* can be established as:

$$L_{\underline{S}}^T = [[-I_3, AS(\underline{X})]; [O_3, -I_3]] \tag{4}$$

Considering for example, the convention of roll (ϕ), pitch (θ) and yaw (ψ) *(RPY)* angles to describe orientation, the previous relation bas to be rewritten using the matrix Ω_{rtl} defined by:

$$\underline{\Omega} = \Omega_{rtl}^{-1} \cdot \begin{pmatrix} \dot{\phi} \\ \dot{\theta} \\ \dot{\psi} \end{pmatrix} = \begin{pmatrix} 0 & -S\phi & C\phi \cdot C\theta \\ 0 & C\phi & S\phi \cdot C\theta \\ 1 & 0 & -S\theta \end{pmatrix} \cdot \begin{pmatrix} \dot{\phi} \\ \dot{\theta} \\ \dot{\psi} \end{pmatrix}$$

In this case, the interaction matrix is expressed by:

$$L_{\underline{S}}^T = [[-I_3, AS(\underline{X})]; [O_3, -\Omega_{rtl}]] \quad (5)$$

In this model, the orientation is decoupled and an exponential decay of the rotation angles can be obtained, but this does not apply to the position of the end effector.

4.2 New model

In this section, a new model for the pose parametrisation (position and the orientation) of the frame object in the sensor frame is presented. The main advantage of this approach is that camera translation control and orientation control are separated.

Considering the scene described by figure 1, without loss of generality the absolute frame can be chosen equivalent to the sensor frame at the equilibrium situation ($\mathcal{R}_A = \mathcal{R}_c^*$). The pose parameters of the sensor frame can be expressed as a rigid transformation matrix $\overline{M}_{(t)} = \begin{bmatrix} R(t) & \underline{x}(t) \\ 0 & 1 \end{bmatrix}$ where $R(t)$ represents the orientation part of the pose, and $\underline{x}(t)$ the position of the sensor frame expressed in the absolute frame. Using the exponential representation, $R(t)$ is expressed by $R(t) = exp(-AS(\underline{\theta}(t)))$ where $\underline{\theta}(t) = \|\underline{\theta}(t)\|.\underline{u}(t)$ is the orientation vector.

Deriving the expression of $\overline{M}(t)$, using $\underline{V}(t)$ as the translation velocity expressed in the sensor frame and $AS(\underline{\Omega})$ as the antisymmetric matrix associated with the rotation velocity $\underline{\Omega}$ expressed in the sensor frame, the following relations can be obtained:

$$\begin{cases} \frac{d}{dt}\underline{x}(t) &= R(t) \,.\, \underline{V}(t) \\ \frac{d}{dt}R(t) &= R(t) \,.\, AS(\underline{\Omega}) \end{cases} \quad (6)$$

In order to transform the relations 6 in the state space formalism, a dimension 6 state vector $\underline{X}(t) = (\underline{x}^T(t), \underline{y}^T(t))^T$ ($\underline{x}^T$ represents the transpose of $\underline{x}$) was chosen.

Developing the exponential representation of $R(t)$ with the Rodrigues formulae [13], $\underline{y}(t)$ is defined by:

$AS(\underline{y}(t)) = \frac{1}{2}(R^T(t) - R(t)) = sin(\|\underline{\theta}(t)\|).AS(\underline{u}(t))$

and its expression is given by the relation:

$$\underline{y}(t) = \frac{sin(\|\underline{\theta}(t)\|)}{\|\underline{\theta}(t)\|}.\underline{\theta}(t) \quad (7)$$

Then, the state equation of the system can be expressed:

$$\frac{d}{dt}\,\underline{X}(t) = B(\underline{X}) \,.\, \underline{U} \quad (8)$$

where $\underline{U} = (\underline{V}^T, \underline{\Omega}^T)^T$ represents the the control vector, and $B(\underline{X}) = \begin{bmatrix} R(\underline{y}) & O_3 \\ O_3 & A(\underline{y}) \end{bmatrix}$ the control matrix with

- $R(\underline{y}) = exp(-\frac{asin(\|\underline{y}\|)}{\|\underline{y}\|}.AS(\underline{y}))$ ($asin$ represents the trigonometric function arcsinus)
- $A(\underline{y}) = -\frac{1}{2}(trace(R(\underline{y})).I_3 - R^T(\underline{y}))$

O_3 and I_3 are the null and identity matrices respectively.

Thus, the state equation of the system is linear with regard to the control vector $\underline{U}$, and non-linear with regard to the state vector. Controllability of the system is obtained if the control matrix $B(\underline{X})$ is full rank. In our case, this condition is always realized except in the singular case $\|\underline{\theta}\| = \frac{\pi}{2} + k\pi$.

In the conditions used in all theoretical development ($0 \leq \|\underline{\theta}\| < \frac{\pi}{2}$), the inverse of the control matrix $B(\underline{X})$ can be computed, and its expression is:

$$B^{-1}(\underline{X}) = \begin{bmatrix} R^T(\underline{y}) & O_3 \\ O_3 & A^{-1}(\underline{y}) \end{bmatrix} \quad (9)$$

To control the system, a non-linear state feedback which linearises the closed loop system is given by:

$$\begin{cases} \underline{U} &= -B^{-1}(\underline{X}).K.\underline{X} \\ \frac{d}{dt}\underline{X} &= -K.\underline{X} \end{cases} \quad (10)$$

5 Comparison of the two approaches

Before addressing the comparison, it is necessary to number the control laws, as defined in the following table:

Law	Approach	Features	Gain
1	Image based	$2D$ points	$\lambda = 0.625$
2	Position based	$3D$ points	$\lambda = 0.625$
3	Position based	Pose RPY	$\lambda = 0.625$
4	Position based	Pose *new*	K = 0.625 I_6

When the image jacobian is evaluated at the equilibrium, index a is used, and if it is evaluated at each iteration, index a is replaced by index b.

5.1 Theoretical results

We now analyse the convergence and stability of the control laws and then go on to discuss the problems which can be encountered when using a Pose estimation algorithm from image features.

Laws 1-a, 1-b, 2-a and 2-b Considering the task function $e = \hat{L}^{T^+}.(\underline{s} - \underline{s}^*)$, and an exponential decay of this function, a necessary condition to ensure the convergence and stability of the control law is given by: $\hat{L}^{T^+} \,.\, L > 0$.

Practically, except in rare cases, due to the complexity of the computation [2] this condition cannot be evaluated.

Near the equilibrium situation, the condition above can be verified, but no theoretical results are known. The robustness of this assumption under conditions far from equilibrium remains unproven. In this case, it is better to calculate the *interaction matrix* at each iteration than at equilibrium.

Laws 3-a and 3-b Due to the structure of the interaction matrix, the condition $\hat{L}^{T^+} . L > 0$ is always verified.

Law 4 To control the system, a non-linear state feedback which linearises the closed loop system was chosen. In these conditions, to stabilise the system it is sufficient to choose the control gain matrix K as a diagonal matrix with positive values. The closed loop system behaves as a set of decoupled integrators, and each component of the state vector shows an exponential decrease.

Pose estimation To estimate the pose parameters for 3D objects by monocular vision, many methods are proposed in the literature. Some methods give closed form solutions of the inverse perspective problem addressed, the others uses iterative processes to reach the solution. The problem of unicity for the solution is often omitted, and the authors use spatio-temporal filters to extract the right solution. At present, the stability and the convergence towards the right solution (avoiding local minima) of pose measurement is not invariably demonstrated. However, some authors have addressed problems of this kind and some results are known. Similar problems were found when using the *Image Based Approach* as presented by F. Chaumette in [2]. In our application, the use of the DeMenthon algorithm [5] and the choice of the best matching using a spatio-temporal filter was preferred. For the moment, no problems have been encountered, but this is not a theoretical proof.

Figure 2: Camera views for *Positions 1 and 2 and 3*

5.2 Experimental results

Our experimental platform is composed of a Cartesian robot and a parallel vision system called *Windis*. In the experimental tests, two main positioning tasks are first considered: move back (*Test 1*) and forward (*Test 2*) from two Cartesian positions (*Position 1* and *Position 2*). Secondly (*Test 3*), two positions (*Position 3* and *Position 1*) are chosen to show the output of the camera field when using certain control laws. Figure 2 represents the image in the different positions used during the tests (*Position 1*, *Position 2* and *Position 3*).

The different positions are learned by using the non-linear feedback control law with the following initial and final positions:

Tests	**Initial** (m,°)	**Final** (m,°)
1	$(0, 0, 0.5, 0, 0, 0)$	$(0, 0, 1.2, 10, -10, -30)$
2	$(0, 0, 1.2, 10, -10, -30)$	$(0, 0, 0.5, 0, 0, 0)$
3	$(0.15, 0.05, 1.2, 10, -10, -30)$	$(0, 0, 0.5, 0, 0, 0)$,

In this table, position is given in metres, and orientation (roll, pitch and yaw angles) in degrees.

Test 1 and Test 2 First, figures 3 and 4 present the camera frame trajectories in object frame obtained with all control laws. Certain control laws tend to follow a straight line between initial and final positions and the trajectory of the others is affected by the coupling between translation and rotation. The greatest deviation from the straight line is observed when using Law 1-b, due to the control being expressed only in the image space.

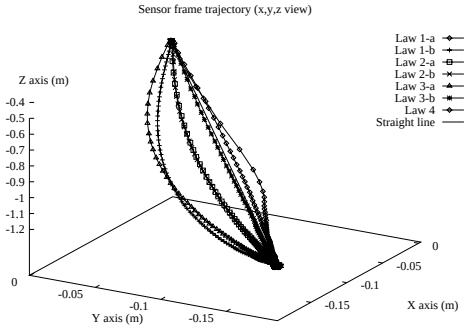

Figure 3: Camera frame trajectories - Test 1

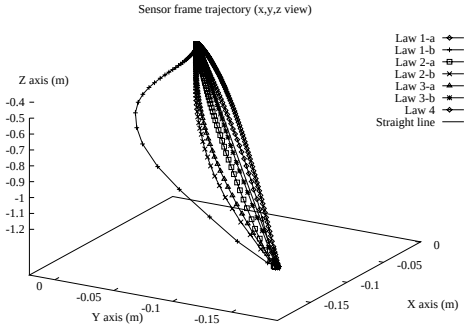

Figure 4: Camera frame trajectories - Test 2

In figures 5-8, the evolution of the projection of the four characteristic points in the image plane is presented. For each control law, the left plot *(1/3)* presents the results corresponding to *Test 1*, and the right plot *(2/4)* those corresponding to *Test 2*.

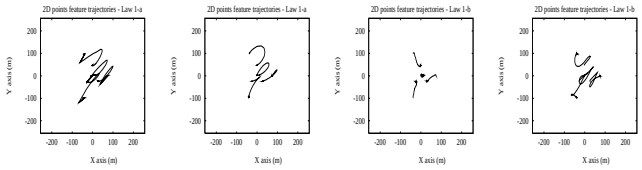

Figure 5: Laws 1-a *(1-2)* and 1-b *(3-4)*

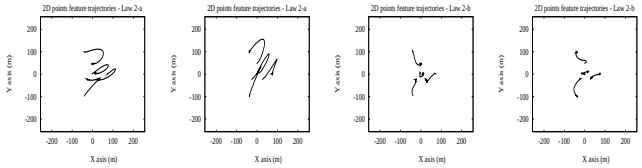

Figure 6: Laws 2-a *(1-2)* and 2-b *(3-4)*

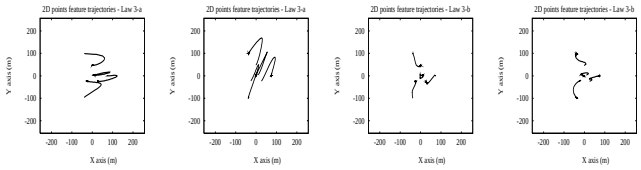

Figure 7: Laws 3-a *(1-2)* and 3-b *(3-4)*

Figure 8: Law 4 *(1-2)*

It appears that the best behaviour is obtained when we compute the interaction matrix at each iteration (Laws 1-b, 2-b and 3-b), except in *Test 2* where Law 1-b uses high velocities.

Overall, the changes in translation and rotation velocities during all servoing tasks is the same (exponential decay). However, for the image based servoing tasks, we have two phenomena. In Test 1, when using Law 1-b the computed velocities are lower than their equivalents for Law 1-a. This is due to the approximation of the interaction matrix. In contrast, in Test 2, translation and rotation velocities are lower when using Law 1-a. These facts explain the deformation of the $2D$ trajectory and $3D$ trajectory (sensor trajectory). As regards the changes in the sensor signals used in the different control laws, an exponential decay can be observed in all cases.

Test 3 In the third test, the initial position is given by *Position 3*, and the final one by *Position 1*. Figure 9 shows the camera frame trajectory during servoing, and the camera view from initial position (*Position 3*). In this test, we compare the behaviour of control laws 1-b, 3-b and 4. As we can see, control law 4 is stopped when the object is outside the camera field. In this case, the servoing task cannot be performed properly.

In figure 10, the changes in the projection of the four characteristic points are presented. The best behaviour in image space seems to be with control law 3-b. In control law 1-b, the coupling between rotation and translation velocities is important. This fact can explain the behaviour of the trajectory in the image plane.

6 Discussion

Many people are interested in visual servoing. Until now, Image Based visual servoing has principally been considered. In this paper, a 3D visual sensor elaborating 3D features at video rate (80ms) has been considered. Several *Position based control* laws and an original model for the Pose parameters which simplify the control synthesis have been proposed.

Concerning the problem of convergence and stability, both approaches present problems. In *Image Based Visual Servoing*, the main problem is to be able to verify the stability condition along the trajectory followed by the sensor. One way to solve this problem may be to choose a particular sensor signal and parametrisation to ensure a particular structure of the *interaction matrix*. This property can enable the demonstration of stability and permit a decoupling between rotation and translation velocities. In *Position Based Visual Servoing*, with the proposed control laws, stability can be demonstrated, but another problem appears: the stability of the *Pose estimation algorithm*.

The special characteristic of this kind of *Position Based Visual Servoing* methods appears in the simplicity of the formalism. The control law depends only on the desired and current situations of the observed object. Then, from one application to another, only the pose algorithm has to be modified.

The choice of the frame used to model the interaction between the sensor and the scene is very important. For example, in the non-linear control law, the sensor

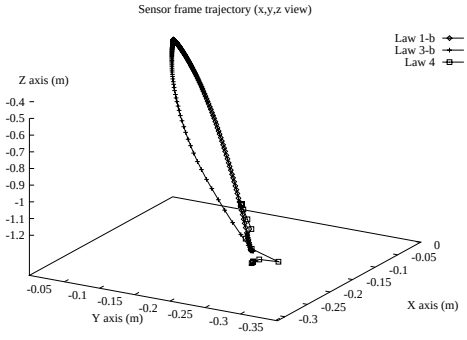

Figure 9: Camera frame trajectories *Test 3*

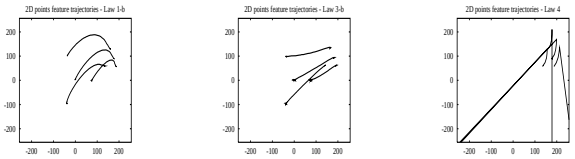

Figure 10: Laws 1-b, 3-b and 4

signal is expressed in the sensor frame at the equilibrium situation. Using this asssumption, the decoupling between translation and rotation velocities is then ensured.

Another important problem is visual feature tracking along an image sequence to ensure matching of the measured feature. For this, three main approaches are possible: independent feature tracking, $2D$ model based tracking or $3D$ model based tracking. Due to lack of information in perspective projection, when ambiguities appear in the image plane, the third method ensures the best tracking.

One question appears through the whole experimental test: how to introduce a constraint into the control law to be sure that the object is always in the camera field during servoing for both approaches.

These results are no more than preliminary. Next, it will be necessary to evaluate the robustness of the control law with regard to noise in pose estimation, modelling errors, and particularly to the hand-eye calibration error.

References

[1] P. K. Allen and A. Timcenko and B. Yoshimi and P. Michelman "Automated tracking and grasping of a moving object with a hand-eye system", *IEEE Transactions on Robotics and Automation*, Vol. 9(2), pp. 152-165, 1993.

[2] F. Chaumette, "Potentiel problems of stability and convergence in image based and position-based visual servoing", *The confluence of Vision and Control*, LNCIS series (237), Springer Verlag, pp. 66-78, 1998.

[3] Corke P., "Visual control of robot manipulators - A review", *in "Visual Servoing"*, Hashimoto K., World Scientific, pp. 1-31, 1993.

[4] S. Christy and R. Horaud, "Iterative pose computation from lines correspondences", *Computer Vision and Image Understanding*, vol. 13(1), pp. 137-144, January 1999

[5] Dementhon D.F., L.S. Davis, "Model-Based Object Pose in 25 Lines of Code", *International Journal of Computer Vision*, vol. 15(1-2), pp. 123-141, June 1995.

[6] Espiau B., F. Chaumette, P Rives, "A new approach to visual servoing in robotics", *IEEE Transactions on Robotics and Automation*, vol. 8(3), pp. 313-326, June 1992.

[7] Feddema J.T. and O.R. Mitchell, "Vision-guided servoing with feature-based trajectory generation", *IEEE Transactions on Robotics and Automation*, vol. 5(5), pp. 691-700, October 1989.

[8] Hager G.D., S. Hutchinson, P. Corke, "Tutorial on Visual Servo Control", *IEEE International Conference on Robotics and Automation*, Minneapolis, Minnesota, USA, 22-28 April, 1996.

[9] Khadraoui D., G. Motyl, P. Martinet, J. Gallice, F. Chaumette, "Visual Servoing in Robotics Scheme Using a Camera/Laser-Stripe Sensor", *IEEE Transactions on Robotics and Automation*, vol. 12(5), pp. 743-749, October 1996.

[10] Martinet P., N. Daucher, J. Gallice, M. Dhome. "Robot Control Using 3D Monocular Pose Estimation", *Proceedings of the Workshop on New Trends in Image Based Robot Servoing, IEEE/RSJ International Conference on Intelligent Robots and Systems*, Grenoble, France, vol.4, pp. 1-12, September 1997.

[11] Martinet P., D. Khadraoui, J. Gallice. "Vision Based Control Law using 3D Visual Features", *World Automation Congress*, Montpellier, France, Vol. 3, pp. 497-502, May 1996.

[12] Papanikolopoulos N., P.K. Khosla, T. Kanade, "Visual tracking of a moving target by a camera mounted on a robot: A combination of control and vision", *IEEE Transactions on Robotics and Automation*, vol. 9(1), pp. 14-35, February 1993.

[13] Rodrigues O. *"Des lois géométriques qui régissent les déplacements d'un système solide dans l'espace, et de la variation des coordonnées provenant de ces déplacements considérés indépendamment des causes qui peuvent les produire"*, Journal de Mathématiques pures et appliquées, Tome 5, pp.380-440, 1840.

[14] Samson C., M. Le Borgne, B. Espiau. *"Robot Control : The Task Function Approach"*, Oxford University Press, 1991.

[15] Sanderson A.C., L.E. Weiss. "Image-based visual servo control using relational graph error signals", *Proceedings of the IEEE International Conference on Robotics and Automation*, pp. 1074-1077, 1980.

[16] Wilson W.J., C. C. Williams Hulls, G.S. Bell. "Relative End-Effector Control Using Cartesian Position Based Visual Servoing", *IEEE Transactions on Robotics and Automation*, vol. 12(5), pp. 684-696, October 1996.